

CURRENT DISTRIBUTION DEPENDENCE ON ELECTRIC FIELD IN HELICALLY COILED CARBON NANOTUBES

*Zoran P. Popović**, *Tatjana Vuković*, *Božidar Nikolić*,
Milan Damnjanović, *Ivanka Milošević*

NanoLab, Center for Quantum Theoretical Physics, Faculty of Physics,
University of Belgrade, Studentski trg 12, 11158 Belgrade, Serbia

Abstract: Experimentally is confirmed that helically coiled carbon nanotube (HCCNT) could be used as a small solenoid for generating spatially localized magnetic field. Current distribution during diffusive electronic transport likewise the inductivity of this quantum conductor depends on electric field. Despite slightly lower electron mobility in HCCNTs than that of the straight single wall carbon nanotubes, the coiled nanotubes are attractive for application as nonlinear nano-solenoids. Nonequilibrium electron distribution functions obtained by solving Boltzmann transport equation are used to predict average helical radius of current flow as a function of electric field intensity. Change of spatial distribution of electronic flow with applied electric field is considered and nonlinear inductivity of HCCNT is predicted.

Keywords: helically coiled carbon nanotubes, electron-phonon interaction, inductance.

1. INTRODUCTION

Modern microelectronics requires ultra-small elements with specific performance, like large self-inductance or nonlinear inductance. Helicoidal electron flow through wire with appropriate geometrical parameters, helical diameter and coil pitch, creates magnetic field along helix axis. Superior inductance has been already predicted in Riemann like graphene nanosolenoid [1,2]. Regularly coiled carbon nanotubes are helically shaped carbon structures, nowadays produced very efficiently, and beside their specific mechanical characteristic like superelasticity [3], it is found that they behave as nanosolenoids with extraordinary properties [4,5]. We modeled stable HCCNTs with very various geometrical parameters, and distribution of pentagons and heptagons inserted between hexagons [6]. Most of them, constructed in accordance with the established procedure [7], have small helical and large tubular radius. Based on occupation of certain atomic orbital, current flow is predicted to occur close to the helix axis [8]. Naturally, when electric field is applied along helix axis, electrons propagation along field direction is followed by spinning around it, since HCCNTs mimic nanosolenoid. Nonequilibrium electron distribution varies with field intensity [9,10] and cause spatial shift of current.

2. ELECTRON AND PHONON BANDS

Electronic transport characteristics of NTs are determined from their electron and phonon spectra. HCCNTs and SWCNTs bands are obtained through implementing modified group projector method. Using symmetry based theory ensure efficient optimization of modeled NTs structure, in calculations of electron and phonon dispersion branches and specific properties [11]. Interactions of all valence electrons involved in sp^3 hybridization, necessary for electronic band calculations, are defined via density functional tight binding matrix elements for carbon-carbon atoms [12]. Electron, as well as phonon dispersion branches over reduced Brillouin zone (BZ) are obtained from diagonalization of the appropriate pulled down Hamiltonian [11,6]. Force constants, required for construction of reduced vibrational Hamiltonian, are extracted from Brenner interatomic potential [13] in optimized model of HCCNTs.

3. ELECTRON PHONON INTERACTION

Lattice deformation caused by dynamics of atoms induces deviation of electronic bonds and change of electronic energy. Description of electron-phonon coupling is not a simple task due to the fact

* Corresponding author: zokapop@ff.bg.ac.rs

that very rarely atoms are moved so that symmetry of the system is preserved during oscillations. Moreover, lattice deformations caused by phonon excitations from the middle of BZ are mostly unhomogeneous. Here, this is overcome by treating electron-phonon interaction perturbatively. In accordance with tight binding framework, two independent components of atomic deformation potential vectors are calculated independently, along the bond connecting two carbon atoms and perpendicular to it. Components of atomic deformation potential are obtained as a two-center integrals of involved orbitals and potential variation of a neutral pseudoatom [14], caused by phonon activation responsible for nonhomogeneous deformation of crystal lattice. Interaction of σ and/or π orbitals make independent of-site atomic deformation potentials vectors $\vec{\beta}_y, \vec{\alpha}_y$ grouped to those along the bonds $y = ss, s\sigma, \sigma s, \sigma\sigma, \pi\pi$ and $y = \pi s, s\pi, \sigma\pi, \pi\sigma$ perpendicular to the bond, as well as on-site atomic deformation potentials $\vec{\gamma}_y$ that have nontrivial contribution in electron-phonon interaction, separated to the deformation potentials oriented along the bond $y = s\pi, \sigma\pi, \sigma\sigma, \sigma\sigma$ and perpendicular to the bond $y = s\pi, \sigma\pi$. Expressions for electron-phonon matrix elements (\mathcal{M}) for straight SWCNTs given in [14] are analytically derived under the assumption that

$$\mathcal{M}^{vt_v n}_{\pm}(\mu t_{\mu} m; \lambda t_{\lambda} l) = -A_{vt_v} \mathcal{D}^{vt_v n}(\mu t_{\mu} m; \lambda t_{\lambda} l) \left(\frac{1}{2} \pm \frac{1}{2} + n_{vt_v} \right)^{1/2},$$

where A_{vt_v} and $\mathcal{D}^{vt_v n}$ are normalized amplitude and electron-phonon matrix elements [14]. Sign \pm correspond to the processes of emission/absorption of the phonon whose population is given by equilibrium Bose-Einstein distribution function n_{vt_v} . In order to

$$\begin{aligned} \mathcal{D}^{vt_v n}_{on}(\mu t_{\mu} m; \lambda t_{\lambda} l) &= \sum_{m' n' l'} [\mu |v^* | \lambda^*]_{m' n' l'}^{m n l} \sum_{z', o'; z, o} C_{z', o'}^{(\mu t_{\mu} m)^*} C_{z, o}^{(\lambda t_{\lambda} l)} \sum_{l', g, y} D_{l', l''}^{(\lambda)^*}(g) \left\{ \vec{\alpha}_y(|R_{z, g} - R_{z', g_0}|) \vec{d}_{z', g_0}^{(vt_v n)} \right. \\ &\quad \left. + \vec{\beta}_y(|R_{z, g} - R_{z', g_0}|) \vec{d}_{z, g}^{(vt_v n)} \right\} \end{aligned}$$

and

$$\mathcal{D}^{vt_v n}_{off}(\mu t_{\mu} m; \lambda t_{\lambda} l) = \sum_{m' n' l'} [\mu |v^* | \lambda^*]_{m' n' l'}^{m n l} \sum_{z, o', o} C_{z', o'}^{(\lambda t_{\lambda} l)^*} C_{z, o}^{(\mu t_{\mu} m)} \sum_{z, g, y} \vec{\lambda}_y(|R_{z, g} - R_{z', g_0}|) \vec{d}_{z, g}^{(vt_v n)}$$

where summation with prime geos over different atoms placed at $R_{z, g}$ and R_{z', g_0} , since numerator z counts the symcell atoms. The coefficients $C_{z, o}^{(\mu t_{\mu} m)}$ of the electron wave function $\psi^{\mu t_{\mu} m}$, describe contribution of the orbital o of the atom positioned at R_{z, g_0} (g_0 is a neutral symmetry group element), are obtained by solving eigenproblem of the Hamiltonian of the electronic subsystem. Energy of phonons

selection rules are satisfied. The formula is derived within extended tight binding framework, considering that straight CNT lattice is built from two atoms unit cell. All possible atomic deformation potential matrix element dependencies on the two carbon atoms distance are given in this paper. They are extracted self-consistently from density functional theory, using Kon-Sham potential and atomic wave functions given in [12]. In the follow-up symmetry approach, we derive electron-phonon matrix elements based on previously proposed predictions. Unlike the given formula, for straight SWCNTs, only correlation between single symcell atom described in [15] and its relevant neighbors have been taken into account. The summation over graphene elementary cell is omitted.

In order to derive numerical values of electron-phonon matrix elements the values of energies and eigenvectors of initial and final electron and phonon states that participate in the allowed processes are to be known. According to the previously proposed theory, here are given formulae for electron-phonon matrix elements and strength of electron-phonon coupling derived for many-orbit system, HCCNT. Electron-phonon coupling can be expressed as

facilitate calculation normalized electron-phonon matrix elements could be partitioned into sum of on-site (\mathcal{D}_{on}) and off-site (\mathcal{D}_{off}) contributions, expressed respectively with

impact the amplitude through Bose-Einstein distribution while electron-phonon matrix elements are related to the phonon polarization vectors $\vec{d}_{z, g}^{(vt_v n)}$.

4. ELECTRON TRANSPORT EQUATION

In semi-classical picture, electron dynamics in CNT placed into homogeneous external electric field

(E) directed along the tube axis, can be described as electron propagation along the CNT interrupted instantaneously by emission or absorption of phonon. Nonequilibrium field dependent electron distribution $f(k)$ in conduction bands, obtained from steady-state Boltzmann transport equation solved in

$$\frac{e}{\hbar} E \nabla_k f(k_\lambda) = - \sum_{\mu t_\mu m} \left[W_{\lambda t_\lambda l}^{\mu t_\mu m} f(k_\lambda) (1 - f(k_\mu)) - W_{\mu t_\mu m}^{\lambda t_\lambda l} f(k_\mu) (1 - f(k_\lambda)) \right].$$

An increase of electric field intensity is followed by a deviation of distribution function from the equilibrium. Solution of given Boltzmann equation gives electron population of the conduction bands as at the given values of the applied electric field and temperature. Electron distribution function depends on temperature and on the intensity of the applied field. It can be used to determine drift velocities [10,18], as well as average values of electron

k space, is used to calculate drift velocity [16, 17, 9]. Electron distribution in the presence of uniform electric field oriented along the tube axis is calculated numerically by solving multi-band Boltzmann transport equation given by

spinning radius dependence on E . At low field intensity, only states around Fermi level are significantly occupied. Further electric field tuning causes spreading of distribution over the other conduction bands and filling conducting states far away from Fermi level. Hence, amplifying of E leads to the inter-band electron crossings if the energy conservation law is satisfied and the corresponding selection rule is fulfilled [19].

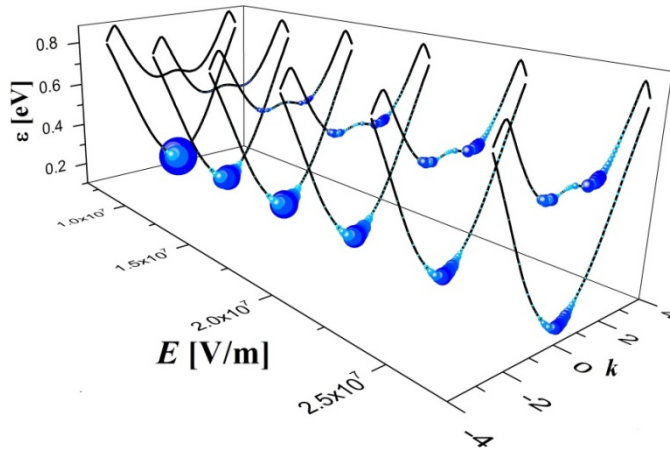


Figure 1. Field dependence distribution of electrons in conducting bands of HCCNT. Population of the states in the band is proportional to the blue bubble size

Electron transition probability per unit time, from the initial state described by $\psi^{\lambda t_\lambda l}(r)$ into the

$$W_{\lambda t_\lambda l}^{\mu t_\mu m} = \frac{2\pi}{\hbar} |\mathcal{M}^{\nu t_\nu n}_\pm(\mu t_\mu m; \lambda t_\lambda l)|^2 \delta(\varepsilon_{\mu t_\mu} - \varepsilon_{\lambda t_\lambda} \pm \hbar\omega_{\nu t_\nu}).$$

Probability of all scattering processes must be included in the Boltzmann transport equation in order to obtain distribution function. Except selection rules, energy conservation must be also fulfilled for the allowed events, followed by emission or absorption of phonons. If selection rules are not satisfied, all matrix elements of a projector $[\mu|v^*|\lambda^*]$ [20] equals to zero, which means that electron and phonon in the given states are not coupled, since the appropriate electron-phonon matrix elements vanish.

final state $\psi^{\mu t_\mu m}(r)$ is evaluated using Fermi golden rule:

The total scattering rate at a finite temperature is obtained summing the contribution of the all permitted scattering events.

High temperature sensitivity of scattering rate appears when low energy acoustic phonons are involved in transition processes. Due to the high intensity of scattering rate at any temperature, electron transitions occur frequently being thus redistributed.

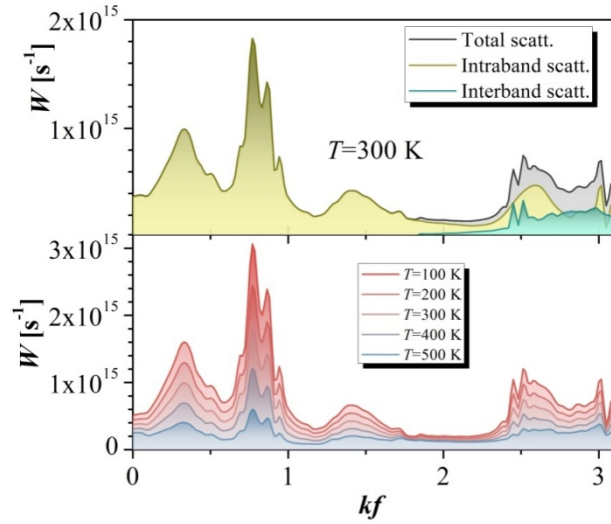


Figure 2. Contributions of interband and intraband processes to the total scattering rate of the states from the lowest conduction band (upper panel) and temperature dependence of their total scattering rate (lower panel), represented in reduced BZ of (5,2,2,2,((1,7),(0,8))) HCCNT

5. CURRENT DISTRIBUTION

Electron flow takes place over atoms whose orbitals largely contribute to the electronic Bloch wave function of the conduction states [21]. When voltage is applied along the helix axis of HCCNT trajectory of helical current flow follows the shape of the tube. Previously presented results show that occupancies of the states in the conduction band vary with intensity of electric field as well as with temperature. Accordingly, electron contribution from different states to total current depends on applied field. Average value of helical radius for electron current, spinning around helix axis, depends on expected values of helical radius ($\bar{\rho}_{vtv}$) of filled electron states and their occupancy $f_{vtv}(E)$. Therefore, it is obvious that average helical radius of elec-

$$\bar{\rho}_{vtv} = \langle \psi^{vtv} | \hat{\rho} | \psi^{vtv} \rangle = \sum_{z,z',g} \sum_n 2\text{Re}[(z'g_0) \langle vt_v n | J_{z,g}^{z',g_0}(\rho) | vt_v n \rangle^{(zg)}],$$

where $J_{z,g}^{z',g_0}(\rho)$ is 4×4 matrix, since prime in the sum means that pairs are not repeated. Elements of J are defined as

$J_{z,g}^{z',g_0}(\rho) = \langle \chi_{oi}(r - R_{z',g_0}) | \hat{\rho} | \chi_{oj}(r - R_{z,g}) \rangle$, where $\chi_o(r - R_{z,g})$ is Slater type orbital for carbon atom positioned at site $R_{z,g}$.

All matrix elements $J_{z,g}^{z',g_0}(\rho)$ are derived numerically, for pairs of atoms of which at least one belongs to the symcell, since the other one could be within the relevant neighborhood, i.e. within the range of the interaction. As a consequence, relation

tron current changes with variation of applied electric field, and the dependence can be calculated using the following expression

$$\rho(E) = \frac{\sum_{vt_v n} \bar{\rho}_{vt_v} f_{vt_v n}(E)}{\sum_{vt_v n} f_{vt_v n}(E)}.$$

Values of expected helical radius for conduction band states must be known in order to determine average radius of the current. For electronic state, described by Bloch function $\psi^{vt_v n}(r)$ expected radius of electronic helical path $\bar{\rho}$ is obtained following quantum mechanical definition. From expression for Bloch wave function [22] rearranging intermediate steps toward the final form applying orthogonality relation, valid for matrix elements of irreducible representation, condense formula for expected values of $\bar{\rho}$ is given as

given for expected radius has finite summation, which goes over several elements of line group or neighbors for each symcell atom. Calculation of expected trajectory radius for electron in certain state for typical HCCNT requires very large number of matrix blocks J , and their numerical evaluation requires significant resources. For instance, finding $\bar{\rho}$ for typical HCCNT with symcell of 108 atoms required calculation of 2019 independent blocks J . Once extracted J matrices for certain NT could be used for finding expected helical radius for each electronic state. Effectively, $\bar{\rho}$ of specified state depends on components contained in electronic

eigenvector associated to the atomic orbital. Radius of electron flow in HCCNT is limited by geometrical parameters of the coiled nanotube. Expected value of helical radius with respect to arbitrary state in HCCNTs fall within wide range, i.e. between the

inner and the outer radius of the tube. Coefficients of eigenvectors change gradually with wave-vector along certain band from electron spectra in BZ as well as $\bar{\rho}$. Function $\bar{\rho}_{vtv}$ is not strictly monotonic over the entire BZ as it is shown in Figure 3.

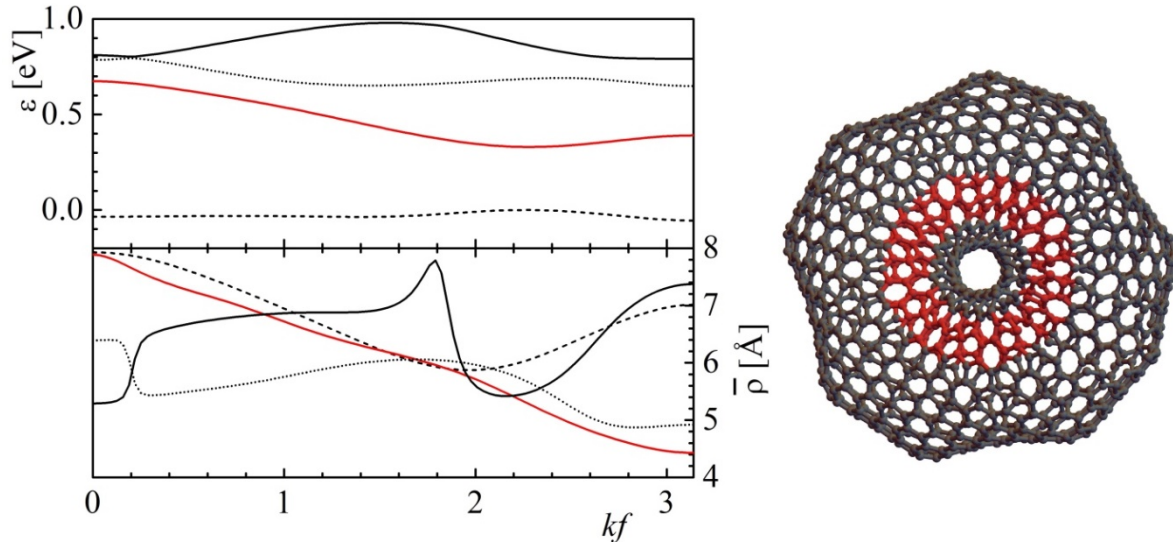


Figure 3. Left: Electronic bands in the Fermi level vicinity (upper panel). Expected radius dependence on the wave-vector, presented like the corresponding bands of the upper panel (lower panel). Right: Atoms red-highlighted are in range of expected values of helical radius (left, lower panel) for red band states (left, upper panel)

In accordance with changes of electron distribution with applied electric field, gradually change of average electron radius versus intensity of applied field also has been predicted. Obtained results show shift of average radius with E in ranges of expected electron radius for the states in conducted bands and reflect their occupation. In the absence of electric field, degenerate states from the same band defined with k and $-k$ would be equally occupied, which affects that equal number of electrons move clockwise and anticlockwise, causing vanishing of magnetic field. Otherwise, depending on the direction of nonzero electric field applied along helix axis, one direction of electron current becomes preferred inducing nonzero total magnetic field. With respect to the exposed, HCCNTs could be considered like nanosolenoids with their own inductance. Generally, inductance of classical solenoid is characterized only with geometrical parameters of the coil and mostly does not change with the current intensity. Effectively, inductance of a particular HCCNT depends on the spatial current distribution along the tube. Accounting all previously mentioned, it is naturally indicated that inductance of HCCNTs together with average helical radius of electron flow depends on applied electric field. This characteristic classified helically coiled nanotubes among nonlinear nanosolenoids, unlike the classical

solenoids whose inductance are mostly insensible to the applied field. Prediction of inductance changing via tuning E for HCCNT, caused by shifting average current radius is indicated.

Average electron helical radius versus E in practical range is analysed for several HCCNTs. At low field, since only intraband electron transitions occur, average radius is changed in accordance with redistribution of conducted electrons, following trend of $\bar{\rho}(k)$ along the same dispersion branch. Positive differential inductance at low field is predicted in all used HCCNTs models, which means that average radius increases with E as shown in Figure 3. For example, when range of applied field belongs to the dashed red rectangle appropriate electron distribution in one of the examined tubes is depicted in Figure 4 b), where light blue bubbles tail gently spread and rise up to the states with larger expected radius as a response to the increasing of E . Further amplification of field induces additional filling of states with significant contribution of interband scattering allowed by energy conservation and selection rules. As a consequence of electron accumulation in a vicinity of local maxima of $\bar{\rho}(k)$ in the upper band, depicted in Figure 4. c), relative change of average radius reaches maximum and continues with opposite trend, that is decreases in the yellow dashed segment given in Figure 4. a).

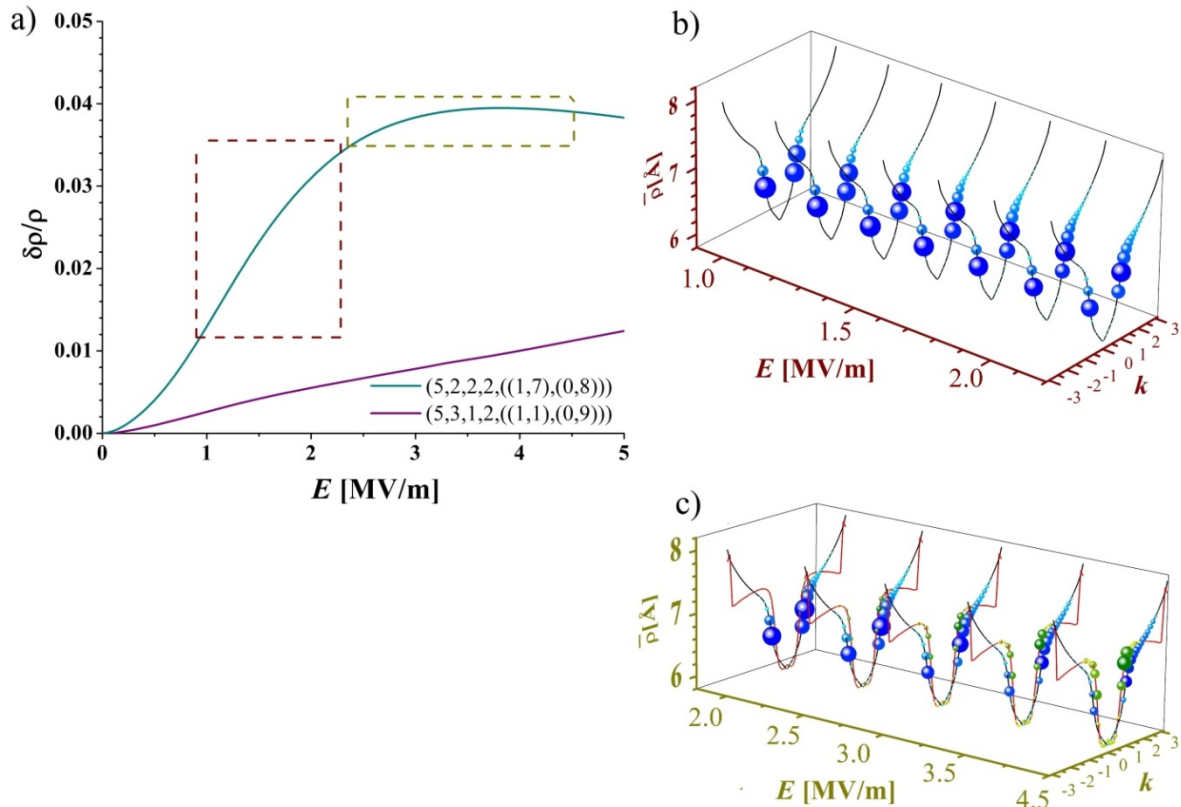


Figure 4. a) Relative change of average radius of electron helical trajectories with regard to radius at $E = 0$ (i.e. in the absence of applied field) as a function of the applied field for two HCCNTs at 300 K. When applied field is in the range from dark red dashed rectangle segment, states with appropriate expected radius are filled like in b) while when E has values from dark yellow segments occupancy of electron states are like in c)

Based on given results, it is predicted that average radius of electron spinning around helix axis can be varied in different manner, which depends on electron structure of used HCCNT and intensity of applied field.

6. CONCLUSIONS

Helical radius of current flow in HCCNTs changes with electric field. This is confirmed on a realistic model, using quantum mechanical techniques. Firstly, all allowed conduction electron scattering channels have been determined together with their probabilities. Then, nonequilibrium electron distribution functions as a solution of the Boltzmann transport equation, are obtained for nanotubes put in an external homogeneous stationary electric field. Electron redistribution with the change of applied electric field is obtained, being effectively manifested through the change of average radius flow. As a consequence of spatial redistribution of current through coiled nanotubes, their inductance can be also tuned with the change of applied electric field.

7. ACKNOWLEDGMENTS

This work is supported by Serbian Ministry of education, science and technology, project OH171035.

8. REFERENCES

- [1] F. Xu, Henry Yu, A.Sadrzadeh, and B. I. Yakobson, *Riemann Surfaces of Carbon as Graphene Nanosolenoids*, Nano Lett. 16, 34–39, (2016).
- [2] S. M. Avdoshenko, P. Koskinen, H.Sevinçli, A. A. Popov, C. G. Rocha, *Topological Signatures in the Electronic Structure of Graphene Spirals*, Scientific Reports, Vol. 3 (2013) 1632.
- [3] L. Zhao Liu, H. Li Gao, J. Jun Zhao, and J. Ping Lu, *Superelasticity of Carbon Nanocoils from Atomistic Quantum Simulations*, Nanoscale Res Lett., Vol. 5–3 (2010) 478–483.
- [4] H. M Faraby, A. M. Rao, P. R. Bandaru, *Modeling High Energy Density Electrical Inductors Operating at THz Frequencies Based on Coiled Carbon Nanotubes*, IEEE Electron Device Lett., Vol. 34–6 (2013).

- [5] K. Yamamoto, T. Hirayama, M. Kusunoki, S. Yang, S. Motojima, *Electron holographic observation of micro-magnetic fields current-generated from single carbon coil*, *Ultramicroscopy*, Vol. 106 (2006) 314–319.
- [6] Z. P. Popović, M. Damnjanović, I. Milošević, *Phonon transport in helically coiled carbon nanotubes*, *Carbon*, Vol. 77 (2014) 281–288.
- [7] I. Laszlo, A. Rassat, *The geometric structure of deformed nanotubes and the topological coordinates*, *J. Chem. Inf. Comput. Sci.*, Vol. 43 (2003) 51924.
- [8] S. Dmitrović, Z. P. Popović, M. Damnjanović, I. Milošević, *Structural model of semi-metallic carbon nanotubes*, *Phys. Status Solidi B*, Vol. 250–12 (2013) 2627–2630.
- [9] V. Perebeinos, J. Tersoff, P. Avouris, *Electron-phonon interaction and transport in semiconducting carbon nanotubes*, *Phys. Rev. Lett.*, Vol. 94 (2005) 086802.
- [10] G. Pennington, N. Goldsman, *Semiclassical transport and phonon scattering of electrons in semiconducting carbon nanotubes*, *Phys. Rev. B*, Vol. 68 (2003) 045426.
- [11] M. Damnjanović, I. Milošević, *Full Symmetry Implementation in Condensed Matter and Molecular Physics Modified Group Projector Technique*, *Physics Reports*, Vol. 581 (2015) 1–43.
- [12] D. Porezag, Th. Frauenheim, Th. Kohler, G. Seifert, R. Kaschner, *Construction of tight-binding-like potentials on the basis of density-functional theory*, *Phys. Rev. B*, Vol. 51 (1994) 12947.
- [13] D. W. Brenner, O. A. Shenderova, J. A. Harrison, S. J. Stuart, B. Ni, S. B. Sinnott, *A second-generation reactive empirical bond order (REBO) potential energy expression for hydrocarbons*, *J. Phys. C*, Vol. 14 (2002) 783.
- [14] J. Jiang, R. Saito, Ge. G. Samsonidze, S.G. Chou, A. Jorio, G. Dresselhaus, and M. S. Dresselhaus, *Electron-phonon matrix elements in singlewall carbon nanotubes*, *Phys. Rev. B*, Vol. 72 (2005) 235408.
- [15] I. Milošević, Z. P. Popović, M. Damnjanović, *Structure and stability of coiled carbon nanotubes*, *Phys. Status Solidi B*, Vol. 249 (2012) 2442–2445.
- [16] D. Querlioz, J. Saint-Martin, P. Dollfus, *Implementation of the Wigner-Boltzmann transport equation within Particle Monte Carlo simulation*, *J. Comput. Electron.*, Vol. 9 (2010) 224–231.
- [17] T. Durkop, B. M. Kim, M. S. Fuhrer, *Properties and applications of high-mobility semiconducting nanotubes*, *J. Phys.: Condens. Matter*, Vol. 16 (2004) R553.
- [18] Z. P. Popović, T. Vuković, B. Nikolić, M. Damnjanović, I. Milošević, *Prediction of electron drift velocity in helically coiled carbon nanotubes*, *Contemporary Materials*, Vol. VII-2 (2016) 116–120.
- [19] Z. P. Popović, T. Vuković, B. Nikolić, M. Damnjanović, I. Milošević, *Transport in helically coiled carbon nanotubes: semiclassical approach*, *Contemporary Materials*, Vol. VI-1 (2015) 15–19.
- [20] M. Damnjanović, I. Milošević, T. Vuković, T. Marinković, *Wigner-Eckart theorem in the inductive spaces and applications to optical transitions in nanotubes*, *J. Phys. A: Math. Gen.*, Vol. 37 (2004) 4059–4068.
- [21] K. Nakada, M. Fujita, G. Dresselhaus, M. S. Dresselhaus, *Edge state in graphene ribbons: Nanometer size effect and edge shape dependence*, *Phys. Rev. B*, Vol. 54, (1996) 17954.
- [22] M. Damnjanović, I. Milošević, *Line Groups in Physics*, Springer-Verlag, Berlin, 2010.



ЗАВИСНОСТ ПРОСТОРНЕ РАСПОДЕЛЕ СТРУЈЕ ОД ЕЛЕКТРИЧНОГ ПОЉА У ХЕЛИКАЛНИМ УГЉЕНИЧНИМ НАНОТУБАМА

Сажетак: Експериментално је показано да се хеликалне угљеничне нанотубе (ХУНТ-е) могу користити као солениоди помоћу којих се генерише просторно локализовано магнетно поље. Просторна дистрибуција електронске струје током дифузног транспорта услед електрон-фонон расејања, а са њом и индуктивност овог квантног проводника зависи од интензитета електричног поља. Упркос нешто мањој мобилности проводних електрона ХУНТ-а у поређењу са правим конвенционалним нанотубама, оне би могле наћи примену као нелинеарни наносолениоди. Неравнотежне дистрибуционе функције, и из њих изведене очекиване вредности хеликалних радијуса усмереног тока кретања електрона добијене су у зависности од интензитета електричног поља. Дата је предикција нелинеарне индуктивности ХУНТ-а.

Кључне речи: хеликалне угљеничне нанотубе, електрон-фонон интеракција, нелинеарна индуктивност.

